

Modelling the 3D vibration of composite archery arrows under free-free boundary conditions

Abstract

Archery performance has been shown to be dependent on the resonance frequencies and operational deflection shape of the arrows. This vibrational behaviour is influenced by the design and material structure of the arrow, which in recent years has progressed to using lightweight and stiff composite materials. This paper investigates the vibration of composite archery arrows through a finite difference model based on Euler-Bernoulli theory, and a 3D shell finite element modal analysis. Results from the numerical simulations are compared to experimental measurements using a Polytec scanning laser Doppler vibrometer (PSV-400). The experiments use an acoustically coupled vibration actuator to excite the composite arrow with free-free boundary conditions. Evaluation of the vibrational behaviour shows good agreement between the theoretical models and the experiments.

Keywords

finite difference modelling, finite element modelling, composite archery arrow, modal response, laser vibrometry

1 INTRODUCTION

Archery is one of the oldest sporting activities undertaken by humans and has long been an area of great interest for engineers. The first documented investigation of arrow mechanics by Leonardo da Vinci shows a centre of gravity applied to the dynamics of arrow flight [1]. The performance and design of modern archery equipment has advanced as manufacturers have made incremental improvements to the mechanical components of both bows and arrows. In recent years the use of theoretical modelling has been applied to the bow and arrow system to better understand the dynamic performance as detailed in previous publications [2, 3, 4, 5, 6, 7, 8]. In this paper finite difference and finite element (FE) modelling of composite arrows with free-free boundary conditions are analysed and compared to experimental results to determine the accuracy of modelling the vibrational behaviour of arrows.

Understanding the mechanical system of the bow and arrow is one of the factors noted by Axford [2] that is required in archery performance. The dynamic behaviour of interest includes the two phases of the shot, that is the power stroke as force is imparted to the arrow by the bow, and the free flight of the arrow influenced by aerodynamic drag. It is inevitable that an arrow will flex both during the bow's power stroke and then also as it moves from the bow towards the target as documented by Zanevskyy [3]. Aside from the substantial forces from the string accelerating it up to speed, the bow's nocking point (where the arrow is attached during the power stroke) moves both in the

vertical and horizontal planes during the power stroke, applying substantial lateral forces to the arrow. For a recurve bow the movement in the horizontal plane is due to the manner in which the string leaves the archer's fingers. In the vertical plane the nocking point moves laterally due to the arrow being usually placed above the geometric centre of the bow. Pekalski [4] and later Kooi and Sparenberg [5] modelled the arrow flexing during the power stroke of a recurve bow, solving the equations of motion using the implicit backward Euler and Crank-Nicholson methods. For a compound bow the movement in the horizontal plane is largely due to the lateral forces from the bow's cables on the cable guard and in the vertical plane it is due to the bow's cam design. Park [6,7], used the Kooi and Sparenberg technique, but with an explicit finite difference scheme, to model the behaviour of an arrow both during the power stroke of a compound bow and then the arrow's behaviour in free flight.

It is necessary to have the arrow flex in order for it to pass the support on the bow's handle section without the rear of the arrow making contact and thus disturbing the path of the arrow. The flexural rigidity of the arrow should allow one full cycle of oscillation by the time it leaves the bow. Klopsteg [8], using high-speed flash photography, demonstrates the manner in which an arrow flexes as it passes around the handle section of a longbow. Following Klopsteg's work, Nagler and Rheingans [9] provide a mathematical basis for selecting the stiffness of an arrow to match a particular bow. This selection of arrows is directly applicable to the wider sporting community. Current

methods that are employed to match the arrow to the bow involve using an arrow selection chart supplied by the manufacturers [10]. The selection chart gives a range of arrows that are suitable for both recurve and compound bows. The chart is a matrix of arrow length versus bow weight in five-pound draw force increments. While this selection chart is a reasonable starting point for matching arrow to bow, current methods require fine-tuning through a process of trial and error to refine the size of the arrow groups on the target. This process could be improved by modelling the arrow to provide a more precise match of arrow to bow. Modelling is also useful for designing archery equipment with better performance, longer product life, and for understanding the structural health of arrows during the effective product life [11].

The flexural behaviour of arrows is not easy to measure experimentally. It is necessary to use either high frame rate video or multiple single frame photographs a method used by Park [6] and also Klopsteg [8] in laboratory conditions. Typically, 4000 frames per second has been necessary to capture sufficient detail of an arrow's behaviour as it leaves the bow vibrating at 80 Hz. However, where available, even moderately expensive video cameras have only limited resolution when used at those frame rates. Nevertheless, and especially for recurve bows (the type used in Olympic Games competition), the manner in which an arrow flexes is of fundamental importance in adjusting the bow such the arrow flies well. Hence, the ability to model this behaviour

mathematically is of interest in assisting archers in optimal equipment selection and adjustment.

This paper presents two alternative methods for accurately modelling the vibratory response of archery arrows in free flight, as well as the experimental validation. The approach used in this research is to compare the results from the finite difference method and the FE technique to experimental measurements for three different types of composite archery arrows. The aim is to validate the theoretical models to give greater confidence in using models to predict the performance of composite arrows. The arrow models may then be used to provide a precise match of arrow to bow for a range of different arrow lengths and bow weights. Such models may also be used as a basis for investigating specific performance requirements such as the aeroelastic behaviour of arrows in flight or the effect of damage in the composite arrows.

2 ARCHERY ARROW SPECIMENS

Arrows most commonly used in major competition are made from tubular carbon fibre composite material bonded to an aluminium inner core. This research investigates three different composite arrow types; namely the ProTour380, ProTour420 and ProTour470 made by Easton Technical Products. These arrows were constructed to the same shaft length of 710 mm, but have a different nominal diameter as shown in Figure 1. Note that the diameter, and hence the mass and stiffness, vary along the arrow's length.

Composite arrows often have a tapered diameter to either the front, or to both the front and the back. This tapering provides the arrow stiffness and aerodynamic characteristics required for competition archery. The static spine of the arrow may be measured as the deflection of the arrow in thousandths of an inch when an 880 gram (1.94 lbs.) mass is suspended from the centre of the arrow supported at two points 711 mm (28 inch) apart [6]. For example, the ProTour380 has a deflection of 9.652 mm (380/1000 inch) when tested for static spine [10]. The static spine test was used for estimating unknown material properties of the composite arrow used in the theoretical simulations.

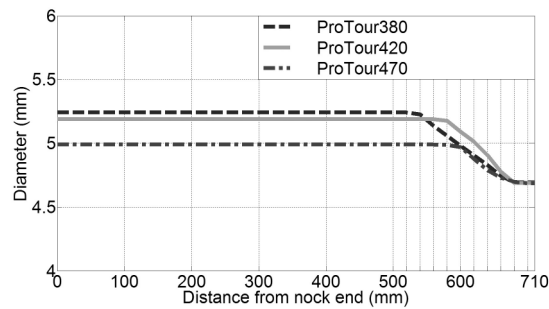


Fig. 1 Measured diameter of arrow specimens

Arrow components including nock, fletching and arrow point must be accounted for in the theoretical models. The nock of the arrow made from polycarbonate plastic, which fastens the arrow to the bowstring, is attached to a small aluminium pin inserted into the arrow shaft. Three fletches made from soft plastic are glued to the rear of the arrow shaft. The point of the arrow made from stainless steel has a long shank that fits inside the arrow shaft as shown in Figure 2. In this work, the arrow nock and fletches had a

combined mass of $m=1.58$ g, and the arrow point mass was $m=7.776$ g. The extra mass from these arrow components was applied in the most appropriate manner to the theoretical models. The finite difference method used lumped masses at appropriate grid points along the beam with the stiffness of the arrow shaft increased at both ends; more so at the front, in view of the nock pin and point shank. The FE technique used two point masses applied at the centre of gravity with mass moments of inertia, one at the front and one at the rear of the arrow as seen in Figure 2. The arrow nock, nock pin and fletches combined had moments of inertia $I_x = 0.034$ kgmm² and $I_y = I_z = 0.59$ kgmm² applied at the centre of gravity $x=15$ mm. The arrow point mass moments of inertia $I_x = 0.0198$ kgmm² and $I_y = I_z = 4.42$ kgmm² applied at the centre of gravity $x=703$ mm from the nock end of the arrow.

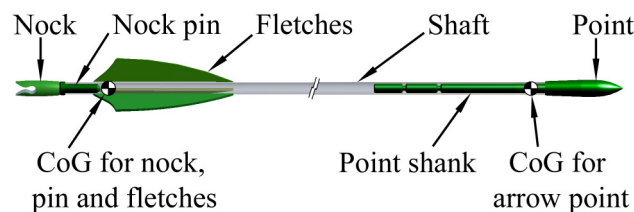


Fig. 2 Composite arrow detailing arrow components, with mass and moment of inertia loading used in FE model applied at the centre of gravity (CoG)

The arrow shaft composite material was made of a core tube of aluminium with an outer layer of carbon and epoxy resin. The core material AL7075-T9 aluminium had an outer diameter of 3.572 mm (9/64 inch), a thickness of 0.1524 mm (6/1000 inch) and a

density of $\rho=2800 \text{ kg/m}^3$. The aluminium had isotropic material properties with Young's modulus of $E=72 \text{ GPa}$ and Poisson ratio of $\nu=0.33$ [12].

The properties of the outer layer of carbon and epoxy resin were estimated from physical measurements along with the static spine of the arrow as quoted by manufacturers. The inner aluminium tube of the arrows has a constant inner and outer diameter. For many arrows the outer layer and hence the thickness of the carbon fibre composite material, varies in thickness. This can be readily measured. The mass of the arrow can also be measured and hence the density of the carbon fibre composite obtained. The static spine test is then performed mathematically using the finite difference method to solve the equations of motion and the flexural rigidity of the carbon fibre composite material adjusted such that the correct static deflection is obtained. Consequently both the density and the flexural rigidity are both then available. The arrows under test have a high proportion of carbon fibre to matrix and have all of the fibres running longitudinally along the arrow shaft (the objective is to have a high shaft stiffness but small diameter). Consequently these arrows can be prone to splitting longitudinally, although the small diameter aluminium core tube does provide some circumferential strength in addition to that provided by the matrix. Larger diameter arrows usually include circumferential as well as longitudinal fibres in order to provide adequate wall strength, although that type of arrow was not the subject of this work. The density and modulus quoted for the composite and is expected to be close to that of the

fibres alone. A density of $\rho=1590 \text{ kg/m}^3$ was used for the matrix, with a Young's modulus of $E_1=222 \text{ GPa}$ in the fibre direction along the arrow shaft. Orthotropic elastic carbon epoxy materials require properties defined orthogonal to the fibre direction. These properties were estimated from similar materials that are transversely isotropic [13,14]. A Young's modulus of $E_2=E_3=9.2 \text{ GPa}$, shear moduli of $G_{12}=G_{13}=6.1 \text{ GPa}$, and Poisson's ratios of $\nu_{12}=\nu_{13}=0.2$ and $\nu_{23}=0.4$ were used. To complete the required nine constants of the orthotropic elastic material, the shear modulus G_{23} was calculated as $E_2/(2(1+\nu_{23}))=3.28 \text{ GPa}$ [15]. It is noted that the estimated material properties might be a source of error that could be reduced using a model update process to gain a closer approximation to the actual physical values [13,16]. The update process was not used in this current research as the first estimation made from physical measurements provided sufficiently accurate results.

3 FINITE DIFFERENCE METHOD

Using the finite difference technique of Park [7], the arrow was modelled as an inextensible Euler-Bernoulli beam with point masses distributed along the shaft. These masses include the nock, fletching and arrow point (as seen in Figure 2). The arrow components that were inserted and glued into the arrow shaft increase the stiffness of the arrow shaft at both ends as shown in Figure 3. The arrow model needs to include these additional masses and increased shaft stiffness.

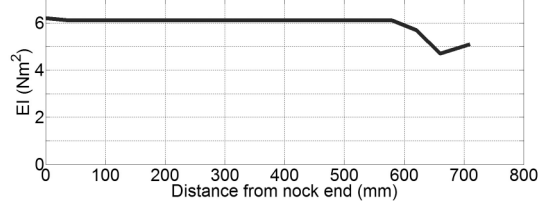


Fig. 3 ProTour420 arrow stiffness along length of shaft

The equations of motion for the arrow were obtained from Newton's second law of motion

$$m_{shaft}(\xi) \frac{\partial^2 \zeta(\xi, t)}{\partial t^2} = - \frac{\partial^2 M(\xi, t)}{\partial \xi^2} \quad (1)$$

and the Euler-Bernoulli beam equation

$$M(\xi, t) = EI(\xi) \frac{\partial^2 \zeta(\xi, t)}{\partial \xi^2} \quad (2)$$

where ξ is the distance from the rear end of the arrow, $m_{shaft}(\xi)$ is the arrow shaft mass per unit length, $\zeta(\xi, t)$ is the deflection of the arrow as a function of time t , $M(\xi, t)$ is the bending moment, and $EI(\xi)$ is the arrow's flexural rigidity.

These equations of motion were then solved using the explicit finite difference method as detailed by Park [7]. For an arrow flexing in free space the boundary conditions are such that the end conditions are free-free giving a shear force of zero at each end of the shaft and the moment at each end of the shaft is zero according to

$$M(0, t) = 0 \quad (3)$$

$$M(L_a, t) = 0 \tag{4}$$

where L_a is the length of the arrow.

The finite difference method only considered the first vibrational mode due to the difficulty of initially deforming the arrow to a shape consistent with the higher modes. Initially the arrow was flexed as it would be under gravity and at time $t=0$ it was released from the effects of gravity. The arrow modelled with no damping then flexes at its natural frequency, which can be measured. The location of the nodes of the fundamental mode of vibration can also be readily obtained and the results are shown in Table 1. It is useful to know the locations of the vibrational nodes for better understanding the behaviour of the arrow as it exits the bow. For these calculations the arrow was modelled as 16 segments, each 44 mm in length, and with time steps of 0.000025 s (40 kHz). Tests for convergence using 32 segments showed that the use of an increased number did not improve accuracy significantly. The time step used in the finite difference method is related to the space step chosen. If the time step is too great for a given space step there is a danger that the explicit finite difference method becomes unstable. Hence the time step was selected to be well away from that danger, although as noted this does mean greater computing time.

Table 1 Natural frequencies of fundamental bending mode calculated using finite difference method, with node locations as distance from nock end of arrow shaft.

	ProTour380	ProTour420	ProTour470
Frequency (Hz)	82.3	80.3	78.4
Rear node location	145 mm	144 mm	143 mm
Front node location	643 mm	645 mm	647 mm

4 FINITE ELEMENT MODEL

Finite element (FE) models were also developed to investigate the modes of vibration of the three composite archery arrows. The arrow was modelled using shell elements as it was intended to also investigate the shell modes of vibration. The shell modes are important in relation to the detection of damage in the composite arrows that are prone to splitting longitudinally along the direction of the carbon fibres. Such damage could be detected from the cylindrical modes of vibration such as circumferential, torsional and breathing modes rather than from the beam vibration modes alone [17, 18]. Details of the cylindrical modes of vibration were not included in the paper as it is the subject of a future publication. The computer package used was ANSYS Workbench 12.1 that provided the SHELL281 element, a multi-layered quadratic shell element of 8 nodes. A single shell element represented the full thickness of the arrow wall with 10 elements around the circumference as shown in Figure 4. The shell element was defined with two layers to account for the isotropic aluminium inner tube and the orthotropic carbon epoxy outer layer. Orthotropic elastic material properties were defined such that the carbon fibre lay unidirectionally along the arrow shaft, with transversely isotropic

properties orthogonal to the fibre direction as detailed in Section 2. The inner diameter of the carbon epoxy layer was taken from manufacturer specifications, while the outer diameter of each arrow specimen was measured (as detailed in Figure 1) to find the thickness of the carbon epoxy layer. The shell body was mapped meshed (typical element aspect ratio 1:1) to give 549 element divisions along the 710 mm shaft of the arrow. A total of 16490 nodes and 5490 elements were used.

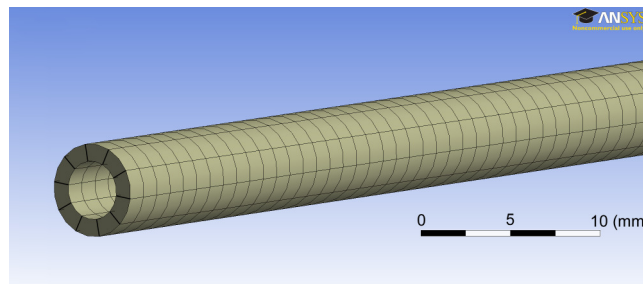


Fig. 4 Meshed arrow

Three FE models were defined to match the physical properties of ProTour380, ProTour420 and ProTour470 composite arrows. Simplifications that were made to the FE models include approximation of the tapered section and use of point masses (including rotational inertia) for the arrow components. The tapered section of the arrow was defined by dividing the shaft length into 50 mm sections each of a different constant thickness. This section length is reasonable given that the finite difference method achieved convergence with similar length segments. The length used results in changes of the outer diameter of no more than 5% per section. The mass of the arrow point, nock and fletches were simplified into two point masses with appropriate mass

moments of inertia, one at the front and one at the rear of the arrow as seen in Figure 2. These point masses and mass moment loadings as detailed in Section 2 were applied with a region of influence over the arrow shaft to replicate the contact area of the arrow components. The region of influence ties the point mass to the arrow shell element nodes to account for the increase in stiffness caused by the shank inserts. It is noted that the small step discontinuities in the thickness and simplified point masses may cause minor discrepancies in the results of the FE models when compared to finite difference models and experimental results.

Eigenvalue modal analyses were conducted using ANSYS to obtain the natural frequencies and mode shapes. The finite element analysis results for the natural frequencies are listed in Table 2. This FE modelling confirmed that the vibrational behaviour was dominated by the bending modes of vibration. Other cylindrical modes of vibration such as circumferential, torsional and breathing modes were insignificant to the overall deflection of the arrow. Comparing the three arrows under investigation the natural frequencies are highest in the ProTour380 and lowest in the ProTour470. This result was expected and is due to the larger diameter and hence greater flexural stiffness of the arrow shaft. The FE technique calculates the minimum and maximum deflection locations at the surface of the shell element. The node locations for the fundamental bending mode were found by observation from the position of the minimum deflection of the arrow shaft.

Table 2 FE results of the first eight natural frequencies, with fundamental node locations at distance from nock end of arrow shaft.

	ProTour380	ProTour420	ProTour470
1 st bending mode with two nodes (Hz)	82.7	81.8	77.6
Rear node location	143 mm	144 mm	139 mm
Front node location	642 mm	640 mm	645 mm
2 nd bending mode (Hz)	249	247	236
3 rd bending mode (Hz)	498	495	475
4 th bending mode (Hz)	819	815	783
5 th bending mode (Hz)	1218	1210	1165
6 th bending mode (Hz)	1700	1687	1624
7 th bending mode (Hz)	2256	2237	2153
8 th bending mode (Hz)	2875	2849	2741

The FE results for the first bending mode of vibration compare favorably to the fundamental bending mode calculated by the finite difference method (shown in Table 1). The greatest difference in the results was seen in the ProTour420 models where the difference in the natural frequency of the fundamental bending mode was 1.5 Hz (2%) and the mode shape front node location was 5 mm different.

5 EXPERIMENTAL TECHNIQUE

Experiments were conducted on the composite arrow specimens using a Polytec PSV-400 3D Scanning Laser Doppler Vibrometer (SLDV). The objective of these experiments was to measure the 3D vibrations of the arrow specimens with free-free boundary conditions, and through those measurements validate the theoretical models. The measurements included the resonance frequencies and modal loss factors of the first eight bending modes, along with the operating deflection shape of the fundamental bending mode of vibration. The modal loss factor is a measure of the damping in each mode and this damping changes the resonance frequency of a structure as detailed later in Eqn (6). If the modal loss factors are small the calculated natural frequencies are approximately equal to the measured resonance frequencies. Details of the experimental apparatus, the SLDV settings, along with the experimental process and results are presented in this section.

The experimental apparatus shown in Figure 5 included a frame to support the composite arrow and two acoustically coupled vibration actuators. The support frame consisted of an optical breadboard with many mounting positions to accommodate the different test specimens. The arrow was suspended horizontally by light elastic cords positioned at the first bending node locations to minimise the effects of additional mass or damping in the connections to the specimen. The vibration actuation was designed to be non-contact by using an acoustically coupled source. The acoustic actuators were a

compression driver from a 50 W TU-50 horn speaker with outlet diameter of 25 mm, and a 3 W loudspeaker with an 80 mm diameter diaphragm. The actuators were required to vibrate the arrow specimens at frequencies of between 50 Hz and 4 kHz. The limitation of the acoustic vibration actuators was the diameter of the sound outlet, where a small diameter will tend to excite higher frequency vibrations in the specimen, while a large diameter sound source will tend to excite low frequency vibrations. The coherence between the source signal and the measured vibration indicated that the compression driver was suitable for the frequency range of 1 kHz to 4 kHz, while the loudspeaker produced better coherence in the range of 50 Hz and 1 kHz [11]. Attachments for the acoustic actuators were used to direct the sound field into the test specimen.

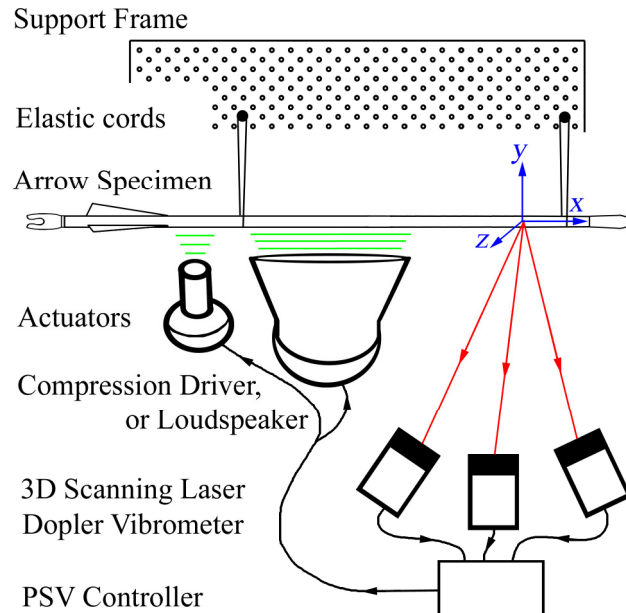


Fig. 5 Experimental apparatus with acoustic vibration actuators

The SLDV used to measure the vibrations operates using the Doppler principle to measure the vibratory velocity in the direction of each laser beam. Laser light from each scanning head was directed at the arrow and a photo-detector recorded the interference of the reflected light with a reference of the original laser light. The Polytec PSV-400 was applied in a 3D configuration using three laser scanning heads to detect the vibrations in three different directions. This 3D configuration provided the data required for the PSV software to perform an orthogonal transformation and calculate the velocity of vibration in three-dimensional space for every point scanned on the surface of the composite arrow. To achieve this the 3D SLDV was aligned such that each laser could scan the entire length of the 710 mm arrow specimens with a recommended laser deflection angle of less than 10°. The lasers were required to be at an optimal standoff distance such that all scan points were within the range 1935 ± 90 mm. When the lasers were positioned, both 2D and 3D alignment procedures are required to align the laser head and video position relative to one another. After the alignment procedures were completed, the error in the positioning of all three lasers on the same point on the arrow surface was found to be less than 1 mm. It is noted that the PSV-400 3D SLDV can be aligned with greater accuracy [19], but for the objective of this experiment higher accuracy was not required.

The PSV software controls the input and output signals of the experiment using the following data acquisition parameters:

1. General: FFT measurement mode with complex averaging of 75.
2. Frequency: Bandwidth of 1 kHz using the loudspeaker and 4 kHz using the compression driver. Experiments used 1600 FFT lines with an overlapping of 75%.
3. Window: The rectangle window function was used for pseudo random generated waveform. The pseudo random signal is periodic in the time window and therefore will generate no leakage effects in the spectrum calculated by the FFT.
4. SE: Signal Enhancement was used for the vibrometer channel, with the speckle tracking turned to a standard level to enhance the signal. Speckle noise occurs from the rough surface of the test specimen that may scatter the laser light. This noise was minimised using signal enhancement as well as ensuring a high degree of reflectivity on the surface of the test specimen using an ARDROX 9D1B reflective surface spray.
5. Vibrometer: The velocity was set to 1 mm/s/V with tracking filter off and the low pass filter set to suit the selected bandwidth.
6. Generator: A pseudo random waveform was used.

The experimental process can be explained by the flow of actuation control and detected measurement signals. The PSV software was used to generate a pseudo random reference signal through a hardware junction box. This signal was connected to an amplifier with a gain of unity, and delivered a voltage to the acoustic vibration actuator to produce the desired excitation in the test specimen. A video camera was used to

coordinate the laser alignment to scan the predefined points on the test specimen. As the three laser heads perform the scan, a velocity decoder (VD-07) provided a voltage proportional to the vibration to a maximum sensitivity of 1 (mm/s)/V. Three signals from the laser heads and the original reference signal are digitised and recorded simultaneously by the computer. The PSV software presented this recorded data in the time domain and in the frequency domain using a Fast Fourier Transform (FFT). A full scan of each test specimen was performed that measured a predefined single line of 25 points along the length of the composite arrow. The time required for each scan depended on the data acquisition parameters selected, and was typically around 20 minutes. Each scan was monitored to ensure good coherence between the generated vibration signal and the measured velocity signal. To get the best coherence for the resonant frequencies measured, the experiments were conducted using both actuators. For the first four bending modes of vibration, the specimens were excited using the loudspeaker, and for the higher modes the compression driver was used.

Experimental results listed in Table 3 show the mean resonance frequencies of three specimens for each type of arrow. The modal loss factor was calculated by the modal bandwidth at a point 3 dB down from the peak of the bending mode frequency and is related to the damping ratio by

$$\eta_b = \Delta f / f_b = 2\zeta_b \quad (5)$$

where η_b is the modal loss factor, Δf is the modal bandwidth, f_b is the mode centre frequency and ζ_b is the damping ratio for bending mode b . The measured frequency response function was between the measured vibration and the excitation voltage signal, and it is assumed in these calculations that there was a flat response between the voltage signal and the force generating the excitation in the arrow. The difference between the calculated natural frequency and the measured resonance frequency can be found by

$$\omega_r = \omega_n \sqrt{1 - 2\zeta_b^2} \quad (6)$$

where ω_r is the resonance frequency, ω_n is the natural frequency and ζ_b is the modal damping ratio. The measured results show a modal loss factor of less than 0.012, thus for these composite arrows each resonance frequency is approximately equal to the corresponding natural frequency.

Table 3 Experimental measurement of resonant frequency f_b and modal loss factor η_b of the tested specimens. Frequency listed as mean \pm standard deviation (Hz).

	ProTour380		ProTour420		ProTour470	
	f_b	η_b	f_b	η_b	f_b	η_b
1 st bending mode (Hz)	83.3 \pm 0.4	0.010	80.2 \pm 0.4	0.007	78.3 \pm 0.4	0.008
Rear node location	142 mm		144 mm		139 mm	
Front node location	636 mm		640 mm		642 mm	
2 nd bending mode (Hz)	248 \pm 0.1	0.005	241 \pm 1.3	0.003	238 \pm 1.7	0.004

3 rd bending mode (Hz)	490±0.7	0.005	478±1.8	0.009	471±4.5	0.012
4 th bending mode (Hz)	795±2.3	0.007	775±4.2	0.004	768±6.4	0.003
5 th bending mode (Hz)	1185±2.9	0.006	1152±3.6	0.004	1144±7.5	0.005
6 th bending mode (Hz)	1663±2.9	0.008	1618±5.0	0.004	1607±7.9	0.005
7 th bending mode (Hz)	2230±2.8	0.007	2165±7.0	0.006	2150±8.7	0.008
8 th bending mode (Hz)	2856±16.5	0.010	2777±12.5	0.007	2761±11.5	0.009
Note: shaded rows show measured results using the compression driver, and unshaded rows show results from the loudspeaker experiments.						

6 DISCUSSION OF RESULTS

A comparison of the arrow mass, natural frequencies and vibratory deflection of the fundamental mode was conducted on results from the theoretical models and the experimental measurements. To compare frequencies, the calculated natural frequency is approximately equal to the measured resonance frequencies since the modal loss factors were between 0.5% and 1.2% as seen in Table 3.

To measure the fit of models to actual arrow specimens, a comparison of the mass of the arrows is shown in Table 4. The arrow specimens were measured using precision scales accurate to 0.01 grams. The theoretical models accounted for the mass of arrow shaft and components in the most appropriate manner for the method used. In the finite difference method the total mass was calculated from the distributed mass along the

arrow. Using the FE technique the total mass was calculated from the density and volume of the shaft materials plus the mass of the nock, fletches and point. There is a small difference between the measured mass of each arrow and the value calculated by the finite difference and FE methods. This discrepancy can be explained by the simplifications such as the definition of the tapered section in the arrow models and any inconsistency in the tapered section of the arrow specimens tested. The arrow specimens are expected to have small manufacturing variations that affect the volume and mass of the carbon epoxy layer of the arrow shaft, for example differences in the outer diameter of the arrow and the position of the tapered section of the shaft.

Table 4 Comparison of measured and calculated mass in grams using different methods

	ProTour380	ProTour420	ProTour470
Measured arrow mass (g)	25.10±0.02	24.81±0.04	23.28±0.02
Finite difference arrow mass (g)	25.20	24.40	23.60
FE calculated arrow mass (g)	25.60	25.32	23.68

A comparison of the measured frequency and the FE predicted frequency for the first eight bending modes of vibration are shown in Figure 6(a). This shows a good correlation for the first eight modes of vibration. The fundamental vibration predicted by both the finite difference and the FE models were compared to the measured frequencies as shown in Figure 6(b). The calculated frequencies of both models were

within 2% of the measured fundamental frequencies for the three different composite arrows tested.

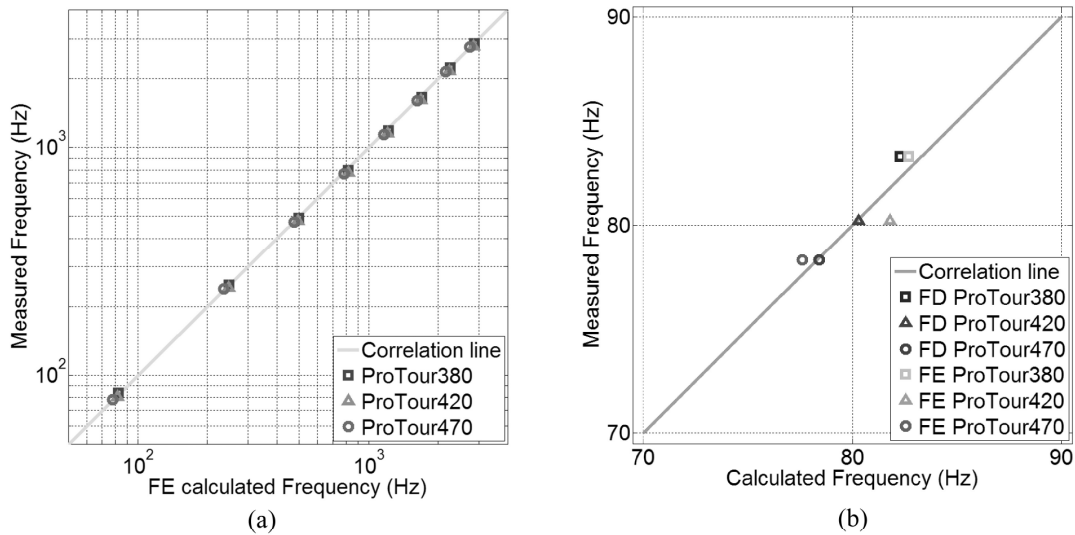


Fig. 6 Comparison of measured and calculated frequencies, (a) first eight bending modes calculated by FE method, and (b) fundamental frequency using both finite difference and FE methods.

The numerically derived mode shapes and operational deflection shape of the fundamental vibration mode for the ProTour420 are shown in Figure 7. The mode shapes were calculated by the finite difference method and the FE technique, where the finite difference method calculated 17 points along the centre line of the arrow, and the FE technique was calculated at 550 points and is shown as a solid line. The magnitude of the calculated lateral displacement is a relative value that has been normalised to unity. The experimentally measured operational deflection shape of the fundamental

vibrational mode was also normalised and is shown as 25 measurement locations on the arrow. These locations were offset a small distance from the nock end of the arrow shaft to allow a good reflective surface for the lasers. The last measurement point was defined on the arrow point just beyond the length of 710 mm arrow shaft. The finite difference lateral displacement diverges slightly toward the point end of the arrow where a small disparity in the definition of tapered section of the arrow will affect the mode shape calculation. This small difference is also seen in the node locations as listed in Tables 1, 2 and 3. The locations of the nodes in Figure 7, shown as locations of zero displacement, are within 5 mm indicating a close correlation between theoretical models and the experiments for the ProTour420.

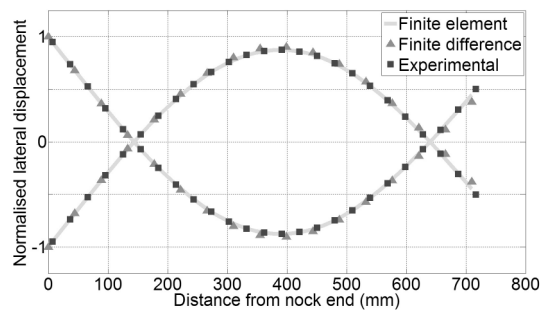


Fig. 7 Lateral displacement comparison of first bending mode for ProTour420

7 CONCLUSION

This paper has compared the results from the finite difference method and the FE technique to experimental results for three different composite archery arrows. The finite difference method was used to solve equations of motion and find the

fundamental mode of vibration for an arrow flexing in free space. The FE technique investigated the modes of vibration up to the eighth bending mode. Experiments were conducted to measure the three dimensional vibrations of the arrow specimens and determine the resonance frequencies and operational deflection shapes of the bending modes of vibration. The theoretical models of these composite archery arrows with free-free boundary conditions have shown excellent correlation to the experimental measurements. The validation that has been performed by this research gives greater confidence in applying these theoretical modelling methods to predict composite arrow performance. The arrow models can be used to assist archers in optimal equipment selection as well as investigate specific performance requirements such as the aeroelastic behaviour of arrows in flight or the effect of damage in the composite arrows.

ACKNOWLEDGMENT

The authors acknowledge the support of Easton Technical Products, who donated arrow products for this research. The assistance from Dorothy Missingham who provided technical writing advice is acknowledged.

© Authors 2011

REFERENCES

- 1 **Foley, V. and Soedel, W.** Leonardo's contributions to theoretical mechanics. *Scientific American*, 1986, **255**(3), 108-113.
- 2 **Axford, R.** *Archery Anatomy*, 1995, pp. 40-63 (Souvenir Press, London).
- 3 **Zanevskyy, I.** Lateral deflection of archery arrows. *Sports Engineering*, 2001, **4**, 23-42
- 4 **Pekalski, R.** Experimental and theoretical research in archery. *J. Sports Sci.*, 1990, **8**, 259-279.
- 5 **Kooi, K. W. and Sparenberg, J. A.** On the mechanics of the arrow: the archer's paradox. *J. Engng Math.*, 1997, **31**(4), 285-306.
- 6 **Park, J. L.** The behaviour of an arrow shot from a compound archery bow. *Proc. IMechE, Part P: J. Sports Engineering and Technology*, 2010, **225**(P1), 8-21. DOI:10.1177/175433711JSET82.
- 7 **Park, J. L.** Arrow behaviour in free flight. *Proc. IMechE, Part P: J. Sports Engineering and Technology*, 2011, DOI:10.1177/17543371111398542.

- 8 **Klopsteg, P.E.** Physics of bows and arrows. *Am. J. Phys.*, 1943, **11**(4), 175-192.
- 9 **Nagler, F.** and **Rheingans, W. R.** Spine and arrow design. *American Bowman Review*, 1937, June-August.
- 10 **Easton Technical Products** 'Easton Target 2011', *Target Catalogue*, <http://www.eastonarchery.com/pdf/easton-2011-target-catalog.pdf> (2011, accessed May 2011).
- 11 **Rieckmann, M., Codrington, J. and Cazzolato, B.** Modelling the vibrational behaviour of composite archery arrows. *Proceedings of the Australian Acoustical Society Conference*, Australia, 2011
- 12 **Gere, J. M.** *Mechanics of materials*. 5th ed., 2001 (Nelson Thornes, London, UK).
- 13 **Lauwagie, T., Lambrinou, K., Sol, H. and Heylen, W.** Resonant-based identification of the Poisson's ratio of orthotropic materials. *Experimental Mechanics*, 2010, **50**, 437-447.
- 14 **Kuo, Y.M., Lin, H.J., Wang, C.N. and Liao, C.I.** Estimating the elastic modulus through the thickness direction of a uni-direction lamina which possesses transverse

- isotropic property. *Journal of reinforced plastics and composites*, 2007, **26**(16), 1671-1679.
- 15 **Craig, P. D. and Summerscales, J.** Poisson's ratios in glass fibre reinforced plastics. *Composite Structures*, 1988, **9**, 173-188.
- 16 **Ip, K.H., Tse, P.C. and Lai, T.C.** Material characterization for orthotropic shells using modal analysis and Rayleigh-Ritz methods. *Composites Part B*, 1998, **29B**, 397-409.
- 17 **Ip, K.-H. and Tse, P.-C.** Locating damage in circular cylindrical composite shells based on frequency sensitivities and mode shapes, *European Journal of Mechanics, A/Solids*, 2002, **21**, 615-628.
- 18 **Royston, T. Spohnholtz, T. and Ellingson, W.** Use of non-degeneracy in nominally axisymmetric structures for fault detection with application to cylindrical geometries, *Journal of Sound and Vibration*, 2000, **230**, 791-808.
- 19 **Cazzolato, B. Wildy, S. Codrington, J. Kotousov, A. and Schuessler, M.** Scanning laser vibrometer for non-contact three-dimensional displacement and

strain measurements, *Proceedings of the Australian Acoustical Society Conference*, Australia, 2008.

APPENDIX

Notation

b	bending mode number
E	Young's modulus
EI	flexural rigidity
f	resonant frequency in hertz
f_b	mode centre frequency
G	shear modulus
I_x, I_y, I_z	mass moments of inertia
L_a	arrow length
m	mass of arrow components
m_{shaft}	arrow shaft mass
M	bending moment
t	time
x	abscissa of the fixed coordinate system
y	ordinate of the fixed coordinate system
z	applicate of the fixed coordinate system
Δf	modal bandwidth

ζ	deflection of the arrow
ζ_b	modal damping ratio
η	modal loss factor
η_b	bending mode loss factor
ν	Poisson's ratio
ξ	distance from the rear end of the arrow shaft
ρ	density
ω_n	natural frequency in radians per second
ω_r	resonance frequency in radians per second